Manuscript prepared for Atmos. Chem. Phys.
with version 5.0 of the LaTeX class copernicus.cls.
Date: 27 August 2014

Systematic satellite observations of the impact of aerosols from passive volcanic degassing on local cloud properties

S. K. Ebmeier[1], A. M. Sayer[2], R. G. Grainger[3], T. A. Mather[4], and E. Carboni[3]

[1]COMET, School of Earth Sciences, University of Bristol, Park Street, Bristol, UK
[2]Goddard Earth Science Technology And Research (GESTAR), NASA Goddard Space Flight Center, Greenbelt, MD, USA.
[3]COMET, Atmospheric, Oceanic and Planetary Physics, University of Oxford, Parks Road, Oxford, UK
[4]COMET, Department of Earth Sciences, University of Oxford, South Parks Road, Oxford, UK

Correspondence to: S. K. Ebmeier
(sk.ebmeier@bristol.ac.uk)

Abstract.

The impact of volcanic emissions, especially from passive degassing and minor explosions, is a source of uncertainty in estimations of aerosol indirect effects. Observations of the impact of volcanic aerosol on clouds contribute to our understanding of both present day atmospheric properties and of the pre-industrial baseline necessary to assess aerosol radiative forcing. We present systematic measurements over several years at multiple active and inactive volcanic islands in regions of low present-day aerosol burden. The time-averaged indirect aerosol effects within 200 km downwind of island volcanoes are observed using Moderate Resolution Imaging Spectroradiometer (MODIS, 2002–2013) and Advanced Along-Track Scanning Radiometer (AATSR, 2002–2008) data. Retrievals of aerosol and cloud properties at Kīlauea (Hawai'i), Yasur (Vanuatu) and Piton de la Fournaise (la Réunion) are rotated about the volcanic vent to be parallel to wind direction, so that upwind and downwind retrievals can be compared. The emissions from all three volcanoes, including those from passive degassing, strombolian activity and minor explosions lead to measurably increased aerosol optical depth downwind of the active vent. Average cloud droplet effective is lower downwind of the volcano in all cases, with the peak difference ranging from 2–8 μm at the different volcanoes in different seasons. Estimations of the difference in Top of Atmosphere upward Short Wave flux upwind and downwind of the active volcanoes from NASA's Clouds and the Earth's Radiant Energy System (CERES) suggest a downwind elevation of between 10 and 45 Wm^{-2} at distances of 150–400 km from the volcano, with much greater local (< 80 km) effects. Comparison of these observations with cloud properties at isolated islands without degassing or erupting volcanoes suggests that these patterns are not purely orographic in origin. Our observations of unpolluted, isolated marine settings may capture processes similar to those in the pre-industrial marine atmosphere.

1 Background

1.1 Aerosol Indirect Effects

Aerosols affect the Earth's albedo directly, through the absorption and scattering of solar radiation, and indirectly, by altering the properties of clouds. Elevated levels of aerosol potentially lead to higher number densities of cloud condensation nucleii (CCN), and for a parcel of cloudy air with a fixed mass of water, result in higher droplet concentrations and consequently smaller droplets and higher albedo (Twomey or first indirect effect; *Twomey*, 1977). In addition, smaller cloud droplets may result in the suppression of precipitation and therefore longer cloud lifetime, i.e. higher albedo (second indirect effect, *Albrecht*, 1989), although the importance of this effect is thought to vary between atmospheric regimes (*Stevens and Feingold*, 2010). If the overlying air is sufficiently dry, the evaporation of small droplets in a polluted cloud is enhanced, so that cloud water content decreases as droplet concentrations increase (*Ackerman et al.*, 2004). The presence of aerosol in a cloud may also cause the evaporation of cloud droplets due to aerosol absorption of solar radiation, in addition to several less well-understood perturbations to droplet character in mixed phase clouds (e.g. *Hansen et al.*, 1997). The impact of secondary aerosol indi-

rect effects have not been well quantified or verified by observations (*Rosenfeld et al.*, 2014).

Aerosol indirect effects (AIE) encompass the combined effects of both anthropogenic and natural emissions. The contributions of AIE to the Earth's radiative balance are strong, yet also highly uncertain. *Carslaw et al.* (2013) suggest that 45% of variance in post-1750 aerosol forcing (the contribution of aerosols to the change in the Earth's radiative balance as CO_2 levels rise) is from natural sources, which are hard to isolate and measure in the polluted present-day atmosphere (*Andreae et al.*, 2007). The response of cloud properties to additional CCN is non-linear: excess CCN has the greatest effect on albedo when background levels of aerosol are lowest (e.g. *Lohmann et al.*, 2005). Present day AIE are therefore expected to most closely match pre-industrial processes in remote marine environments where pollution levels are low (*Andreae et al.*, 2007).

Direct observations of the local effects of aerosols on clouds have so far been dominated by measurements of ship tracks (e.g. *Durkee et al.*, 2000; *Ackerman et al.*, 2000; *Campmany et al.*, 2009; *Christensen and Stephens*, 2011). Ship tracks provide an ideal experiment for isolating the impact of aerosols, as the polluted clouds are similar in origin and thickness to clean clouds in the surrounding cloud deck, although they may be elevated in height (*Christensen and Stephens*, 2011). The occurrence and albedo of ship tracks has been shown to depend on pre-existing cloud structure, height and humidity (e.g. *Chen et al.*, 2012). However, *Peters et al.* (2011) found no statistically significant impact of aerosol from shipping on a large scale, away from the ship tracks themselves.

1.2 Volcanic aerosol indirect effect

The impact of volcanogenic aerosol on cloud properties depends on injection height into the atmosphere, pre-existing aerosol burden and synoptic conditions. Explosive eruptions can inject aerosol directly into the stratosphere (as coarse particles from fragmented magma, vent wall erosion and condensation of magmatic gases) and provide the gas-phase reactants for the production of finer aerosols in the plume or ambient atmosphere (e.g. sulphate aerosol). Direct and indirect aerosol effects associated with explosive eruption products in the stratosphere have been relatively well characterised (*Sassen*, 1992; *Robock*, 2002; *Schmidt et al.*, 2010). However, the role of aerosol in the troposphere from 'passive' degassing and minor eruptions is less well understood (*Mather et al.*, 2003; *Oppenheimer et al.*, 2011). Time-averaged emissions from passive degassing are thought to make up a high proportion (∼30–70%) of the volcanic SO_2 flux to the atmosphere (*Andres and Kasgnoc*, 1998; *Halmer et al.*, 2002; *Mather et al.*, 2003). Volcanogenic aerosols in the troposphere are expected to be dominated by sulphate aerosol (SO_4^{2-}) produced from the oxidation of SO_2 by OH^-, H_2O_2 or O_3 above the boundary layer, or in high temperature reactions of SO_2 or H_2S in the volcanic vent (e.g. *Mather et al.*, 2006). Ambient temperature SO_2 reactions can take place over several days, so the impact of volcanic aerosol on number density of CCN may extend hundreds of kilometres away from the aerosol source (*Eatough et al.*, 1995). Volcanic emissions are one source of natural aerosol that, in combination with anthropogenic aerosol, result in AIE. For readability, we refer to this contribution as 'volcanic aerosol indirect effects' (VAIE).

The flux of volcanic aerosol to the present day troposphere is lower than the anthropogenic flux, but its impact on the radiative budget may be disproportionately significant, as volcanic gases are commonly emitted at heights above the boundary layer into the free troposphere so that aerosol lifetimes may be longer (e.g. *Graf et al.*, 1998). In global model simulations of present-day CCN, uncertainties in volcanic aerosol are lower than those for biomass burning and anthropogenic SO_4^{2-} sources (e.g. *Lee et al.*, 2013). However, volcanic emissions contribute a lower proportion of CCN to the atmosphere today than in pre-industrial times, so the quantification of VAIE are particularly important for estimating the baseline cloud radiative state (*Schmidt et al.*, 2012). Volcanic SO_2 emissions have the greatest potential range of all the natural emissions required to estimate global mean forcing uncertainty (*Carslaw et al.*, 2013).

Ground-based measurements of plumes near passively degassing vents have captured (1) an abundance of SO_4^{2-} aerosol larger than the critical diameter to act as a CCN at typical supersaturations (e.g. *Allen et al.*, 2002; *Martin et al.*, 2008; *Mather et al.*, 2012) and (2) particle growth attributed to the condensation of water vapour onto sulphate particles between 0 and 20 km distance from the vent (Villarica, Chile; *Mather et al.*, 2004). Satellite remote sensing studies have gone a step further to measuring VAIE during periods of high flux degassing. *Gassó* (2008) shows alteration to stratocumulus properties ('volcano tracks') in Moderate Resolution Imaging Spectroradiometer (MODIS) and Advanced Microwave Scanning Radiometer - Earth Observing System (AMSR-E) images where large plumes from volcanoes in the South Sandwich islands and the Aleutians interact with marine boundary layer clouds. Instances of increased cloud brightness in the presence of an obvious volcanic plume were identified by browsing MODIS visible images from six months in 2006, and cloud property data from a few selected days were analysed to demonstrate first and second AIE in the volcano tracks. *Yuan et al.* (2011) have also assessed the impact of high degassing flux associated with a new vent opening at Halema'uma'u crater, Hawai'i, in 2008 on trade cumulus clouds. The authors compare retrievals of cloud and aerosol properties averaged over three months from inside the Halema'uma'u plume to properties both outside the plume over the same time, and to the average properties retrieved over a much longer period. Both studies

(*Gassó*, 2008; *Yuan et al.*, 2011) find evidence for increased albedo and for increased cloud lifetime in marine clouds.

1.3 Motivation and Aim

Although volcanic aerosol acting as CCN has been observed at several volcanoes (e.g., *Mather et al.*, 2004; *Gassó*, 2008; *Yuan et al.*, 2011), its net effect has not previously been quantified over extended periods of time. More representative measurements are important for testing and verifying the predictions of global microphysical aerosol models (e.g. *Martin et al.*, 2006; *Dentener et al.*, 2006; *Schmidt et al.*, 2012), that rely on inventories of sulphur emission such as the one compiled by *Andres and Kasgnoc* (1998).

As measurements of VAIE so far have been made over short time intervals (3-5 months) and during elevated activity (e.g. frequent MODIS thermal anomalies at Montagu and Saunders Islands, *Gassó* (2008); Halema'uma'u vent opening *Yuan et al.* (2011)), they are not likely to be representative of the long-term impact of 'background' activity on tropospheric cloud properties.

This study presents an approach for detecting VAIE for the particular case of isolated, active volcanic islands. We use averages of 6–10 years of data and make no selection on the basis of activity, so that our results may be considered representative of the net effect of volcanic emissions on clouds at a particular volcano. Three 'control' islands (no volcanic aerosol) are also considered, to provide a comparison with possible island (e.g. orographic) effects on cloud properties. Our aim is to capture the VAIE associated with 'background activity', that is, periods when degassing or other persistent activity results in aerosol emission into the troposphere and that may not result in visibly identifiable 'volcano tracks'.

2 Satellite data

Our analysis uses satellite-retrieved aerosol and cloud properties, specifically aerosol optical depth (AOD) at 550 nm, cloud midvisible optical depth (COD), and cloud droplet effective radius (CER). Two satellite products are used for each of these quantities. The first is the Collection 6 MODIS Atmospheres Level 2 Joint product (MYDATML2), from the Aqua satellite (data from 2002-2013). These aerosol/cloud data products are described by *Platnick et al.* (2003), *Ackerman et al.* (2008) and *Levy et al.* (2013). MODIS cloud retrievals (resolution 5×5 km^2) are included where the cloud fraction from MODIS cloud product is > 0.2, and Quality Assurance (QA) values are > 0 (removing data where confidence in the retrieval was low). For aerosol retrievals (resolution 10×10 km^2), we also require QA > 0. The second aerosol/cloud data source is the Oxford-RAL Aerosols and Clouds (ORAC) Global Retrieval of Cloud Parameters and Evaluation (GRAPE) dataset, from Advanced Along-Track Scanning Radiometer (AATSR) measurements, from 2002-2008 (*Thomas et al.*, 2009; *Sayer et al.*, 2010, 2011; *Poulsen et al.*, 2012), with data quality-filtered as recommended by the above. Some significant differences in CER between these two datasets were observed by *Sayer et al.* (2011), attributed in part to the different wavelengths used by the retrieval algorithms, and consequent differences in sensitivity to cloud vertical structure (e.g. *Platnick*, 2000).

For both aerosol datasets, we require pixel cloud fraction < 0.8. Although there may be artefacts in AOD retrieved in conditions of broken cloud (e.g. *Quaas et al.*, 2011; *Grandey et al.*, 2013), we use AOD retrievals when cloud fraction is up to 0.8 to maximise the number of retrievals in our analysis. Cloud fraction, cloud top pressure and temperature were used to distinguish between retrievals from different atmospheric heights and under different synoptic conditions. We restrict our observations to liquid water rather than ice clouds (and to data where cloud top pressures were > 440 mb). All properties are resampled to a grid of 10 km resolution to simplify the comparison. Additionally, data were stratified by season to account for potential large-scale differences in aerosol/cloud properties and data sampling rates in different seasons.

We use Clouds and the Earth's Radiant Energy System (CERES) Single Scanner Footprint data (Top of Atmosphere upward Short Wave flux, resolution 20x20 km^2, *Geier et al.* (2003)) to estimate radiative impact separately from these microphysical property retrievals. Although differences in solar zenith (expected to be $<10^\circ$ in all cases and $<5^\circ$ for majority of retrievals) may result in variations in SW flux across the region surrounding the volcano, correlations with either cloud properties or wind direction are improbable and are therefore unlikely to affect comparison of upwind and downwind SW fluxes.

Data are selected within a square of side length 4° (up to 600 km, depending on latitude) centred on the volcanic vent. We then convert the latitude and longitude for each retrieval pixel into polar coordinates with the origin located on the volcano's summit, as recorded in the Smithsonian database (*Siebert and Simkin*, 2002–). Horizontal wind velocity components from the European Centre for Medium-Range Weather Forecasts (ECMWF, ERA-Interim, spatial resolution = 1.5°, e.g. *Dee et al.*, 2011) are used to rotate the aerosol and cloud properties according to wind direction, so that they can be plotted according to their expected position upwind or downwind relative to the volcano. ERA-Interim horizontal wind velocity components (available 5 times per day) are selected for the time of day closest to the satellite overflight. We assume that aerosols and their precursor gases are emitted from each volcano at approximately its summit height, so wind data are selected for a pressure level expected to lie just above this height. The volcano's summit or the most active vent is treated as the origin for rotation because for all cases here, gases were emitted from multiple vents contributing varying proportions of total aerosol emissions.

The resulting averaged images of rotated cloud and aerosol properties allow us to examine systematic trends that are not apparent in the properties retrieved for individual days, or in the average of all our data before rotation. Unlike previous studies at periods of high SO_2 emission (e.g. *Gassó*, 2008; *Yuan et al.*, 2011), volcano tracks were rarely identifiable in individual MODIS visible images or in cloud properties on specific dates. For MODIS and AATSR, retrievals of cloud and aerosol properties are mutually exclusive, as aerosols are retrieved only in clear-sky conditions. CERES Top of Atmosphere (ToA) upward Short Wave (SW) flux is available for both cloudy and clear-sky conditions.

2.1 Choice of targets

We select target volcanoes where retrieval uncertainties are expected to be low, to allow us to identify low magnitude perturbations in cloud properties. Uncertainties in AOD retrieved from MODIS data over land are thought to be on average three times greater than over water, where models of surface reflectance are better (*Remer et al.*, 2005). We therefore focus our study on isolated volcanic islands, avoiding the higher retrieval uncertainties, greater variability in cloud characteristics associated with continents and the systematic dependence of cloud form on wind over coastlines or high topography (e.g. *Brenguier et al.*, 2003). The ideal target is a small and low-lying island volcano, with a high, persistent degassing flux and located a long way from other sources of tropospheric aerosol, such as cities, heavy industry or shipping.

Three isolated, persistently if variably active volcanoes were chosen to test our approach (Figure 1 and Figure 2): Kīlauea (Hawai'i), Yasur (Vanuatu) and Piton de la Fournaise (Réunion). As described above, measurements of a VAIE downwind of Kīlauea during the opening of the new Halema'uma'u vent were previously made by *Yuan et al.* (2011). Although the results presented here are also for mafic, persistently active volcanoes, they capture a range of eruption styles and degassing fluxes (Table 1).

A VAIE is expected to be characterised by a) elevated AOD and b) depressed CER downwind of the volcanic source relative to upwind. However, we also expect an orographic effect over isolated peaks in topography (e.g. *Jiusto*, 1967) to cause a systematic upwind/downwind difference in CER: when moist air is lifted up over an island it expands, cools and condenses, potentially causing precipitation on the windward side of the island. We therefore also consider data for three 'control' islands known not to emit volcanogenic aerosol or precursor gases (Tristan da Cunha in the South Atlantic; Ofu-olosega, American Samoa and Fiji, both in the South Pacific- Table 1), chosen for their similarities in height and diameter to our target volcanoes (Figure 2), and their isolation from other sources of volcanic or anthropogenic aerosol.

3 Results

The differences between upwind and downwind aerosol and cloud properties are much greater at the volcanoes than at the control sites. AOD is elevated, CER suppressed and ToA upward SW flux higher downwind of all three volcanoes (Figures 3, 4 and 5, Table 2). None of the 'control' islands show a notable difference between upwind and downwind properties or a difference in SW flux exceeding $\pm$ 10 Wm^{-2} (Figure 5).

Degassing processes and patterns are notably different at each of the volcanoes, and we discuss results from each volcano below with reference to other measurements of volcanic aerosol and prevailing meteorological conditions (Sections 3.1–3.3).

3.1 Kīlauea, Hawai'i

Kīlauea is the most active of the Hawaiian volcanoes and contributes 4% of the total emissions in *Andres and Kasgnoc*'s (1998) time-averaged compilation of emissions from 49 continuously erupting volcanoes. Activity is effusive, and split between the East Rift zone, where lava effusion has been semi-continuous since 1983, and periodic degassing, lava pond activity and occasional small explosions at the volcano's summit. Prior to 2008 approximately 90% of SO_2 emissions were from the East Rift Zone and between 2002 and the beginning of 2008, average total annual emissions were 6.58 $\times 10^5$ Mg/yr (*Elias and Sutton*, 2012). A comparison of the USGS ground-based spectrometer measurements with MODIS AOD prior to 2008 for days where both measurements were possible (61 days) does not show a relationship between them (Figure 6), perhaps due to the time difference between the measurements, the lag between SO_2 emission and aerosol formation or processes that affect the concentrations of aerosols, such as dilution.

The opening of a new vent at Halemau'ma'u crater in 2008 was accompanied by a rise in total SO_2 flux to 7000 Mg/day, constituting a doubling of annual SO_2 emission rate from 2007 to 2008. Since 2008 summit emissions steadily increased as a proportion of total SO_2 emission from Kīlauea, though total SO_2 emission had dropped to $\sim$ 2000 Mg/day by 2010 (*Elias and Sutton*, 2012). *Yuan et al.* (2011)'s measurements of the Halema'uma'u 2008 plume demonstrate a significant increase in cloud fraction and perturbation to cloud properties a) inside the aerosol plume, relative to outside and b) during elevated emission in 2008, relative to the mean values for the 11 year Terra archive. On 17th July 2008 *Yuan et al.* (2011) found an average background value of CER of 18 μm, reduced to $\sim$13 μm within the aerosol plume 800–1000 km downwind of Kīlauea. We find a similar magnitude of reduction in CER over a much smaller area (just $\sim$70 km downwind) in averaged MODIS data from 2002-2007, when degassing fluxes were lower as well as in the multi-annual average 2002-2013 (Table 2, Figure 3). *Yuan et al.* (2011) found a 20 Wm^{-2} perturbation within the 2008

Halema'uma'u plume. At distances of $\sim$ 150–400 km downwind of Kīlauea we find perturbations of between 20 and 45 Wm^{-2} (mean = 28 Wm^{-2}) between 2002 and 2013, well constrained to a region within $\sim$45° of the downwind direction. Within $\sim$ 80 km of the vent, where many retrievals would have been over Hawai'i island itself, the perturbation is even higher, exceeding 90 Wm^{-2} (Figure 5 a–b).

Sulphates dominate the compositions of aerosols measured at Kīlauea's summit (modal diameter 0.44 μm), and make up $\sim$1% by mass of plume SO_2 concentrations (*Mather et al.*, 2012). *Porter et al.* (2002) made sun photometer and LiDAR measurements of $SO_4{}^{2-}$ 9 km downwind of a vent on the East Rift Zone in 2001 and found an aerosol dry mass flux rate of 53 Mg/day. They inferred a half life of 6 hours for SO_2 in the plume. Assuming an average wind speed of range 5–10 m/s, if correct and broadly applicable in different atmospheric conditions, this implies that SO_2 mass falls below 10% of its original value by a distance of 90–180 km downwind. Our estimations of average AOD place peak values at $\sim$ 100 km downwind of Kīlauea's summit, consistent with oxidation of SO_2 as the primary source of aerosol.

Aerosol plume dispersal in Hawai'i is dominated by relatively stable trade winds from the north-east. Clouds are mostly trade cumuli, which are typically capped by the trade wind inversion at a height of a few kilometres. Although Kīlauea's summit elevation is only 1222 m, it overlaps the lower flanks of the much larger, but less active, Mauna Loa (4170 m). There is a notable difference in the number of MODIS retrievals flagged as cloud downwind relative to upwind (retrievals with cloud fraction >0.2 are shown in Figure 7). More cloud retrievals were made downwind of Kīlauea, with the difference peaking at a distance of about 60 km downwind of the vent. Elevated downwind COD is likely to be associated with both the formation of orographic cloud and the action of volcanogenic aerosol as CCN.

3.2 Yasur, Vanuatu

Yasur is the southernmost of the Vanuatu island arc's active volcanoes and exhibits almost continuous Strombolian to Vulcanian activity in an eruption that has lasted at least 300 years. Magmatic gases, mostly SO_2, are continuously released from three vents in Yasur's crater and typically rise to heights of 700-900 m before being carried to the northwest by trade winds (*Bani et al.*, 2012). Measurements made by *Bani and Lardy* (2007) and *Bani et al.* (2012) on 33 different days between 2004 and 2008 find an average degassing flux of 633 Mg/day SO_2 (standard deviation of daily measurements = 270 Mg/day). *Bani and Lardy* (2007) estimate that in 2004-5 Yasur contributed 1-2% of estimated global time-averaged volcanic SO_2 emissions to the troposphere, close to *Andres and Kasgnoc* (1998)'s estimation of 3% pre-1990s.

The nearest other aerosol sources to Yasur are just under 400 km away, at the volcanoes of Lopevi (156 Mg/day SO_2) and Ambrym (5440 Mg/day SO_2) (*Bani et al.*, 2012). Yasur is close to being a sea-level point SO_2 source, with a summit elevation of just 361 m. We therefore expect any orographic effects to be minimal. There are also no indications of orographic clouds in rotated cloud properties at the small, remote islands in American Samoa (Ofu-olosega, elevation 639 m) used as 'control' sites.

We measure elevated AOD (e.g. seasonal average upwind-downwind difference are 0.03–0.06 for MODIS (Aqua); 0.02–0.03 for AATSR) downwind of Yasur, relative to that upwind. Ground based SO_2 measurements at Yasur have been too infrequent (*Bani et al.*, 2012) to allow a useful comparison with AOD retrieved from MODIS data. There is also a net difference in CER between the downwind and upwind sectors (seasonal average differences are -3 – -4 μm, MODIS; 0 – -4 μm AATSR). Although some of this difference can be attributed to the impact of excess aerosol from Yasur, this is superimposed on a regional trend in aerosol and does not clearly indicate statistically significant AIE. Similarly, the elevation in ToA upward SW flux downwind of Yasur (Figure 5 c–d) is likely to be influenced by regional variation in cloud properties, rather than purely volcanic effects.

3.3 Piton de la Fournaise, Réunion

Piton de la Fournaise, Réunion, differs from the previous two examples in that intra-eruptive SO_2 flux is low (*Khokhar et al.*, 2005; *Di Muro et al.*, 2012). However, Piton de la Fournaise is very active, on average it erupts or experiences an intrusion once every 8 months (*Peltier et al.*, 2009). Eruptions are sometimes associated with measurable SO_2 emission (*Khokhar et al.*, 2005; *Bhugwant et al.*, 2009), and emission is of longer duration during periods of distal lava effusion when lava entering the sea also results in a high flux of water vapour to the atmosphere (e.g. *Gouhier and Coppola*, 2011). Between eruptions, degassing is primarily from low temperature fumeroles and fractures around the active summit crater (*Di Muro et al.*, 2012). Again, unlike Kīlauea and Yasur, these weak emissions are dominated by water vapour, and hydrogen sulphide (H_2S) is the main sulphur species (*Di Muro et al.*, 2012). La Réunion is located near an important shipping lane (*Peters et al.*, 2011), so it is possible that some anthropogenic sources of sulphate aerosol may also be present.

Piton de la Fournaise is the only one of the volcanoes investigated here that is likely to have had a high SO_2 flux associated with explosive eruption. The SO_2 released during the collapse of the Dolomieu crater in April 2007 (estimated to be 935 $\pm$ 244 kilotons by *Gouhier and Coppola*, 2011) rose quickly to heights $>$ 3000 m (above the trade winds), and reached distances of 800-1000 km away from La Réunion within days (*Tulet and Villeneuve*, 2011). Where SO_2 emission accompanies explosions, and aerosol is carried above the trade winds the aerosol and associated impact will be spread over a much greater area. By distances

of $\sim$ 1000 km, the plume from this event reached heights of around 10,000 m above sea level (*Tulet and Villeneuve*, 2011), so aerosol from the plume are only likely to settle out and re-enter the lower atmosphere at great distance from the volcano. Piton de la Fournaise's other six eruptions between 2002 and 2008 (*Siebert et al.*, 2010) were all less explosive, emitting aerosol lower into the atmosphere.

Differences between upwind and peak downwind AOD at Piton de la Fournaise range from 0.01 to 0.08 (MODIS) in different seasons at $\sim$50 km distance from the volcano's summit, while differences in CER are -2 – -10 μm (seasonal and multi-annual mean MODIS and AATSR values shown in Figures 3, 4 and 8.) Peak downwind elevation in ToA upward SW flux is $\sim$ 28 Wm^{-2} at 20 km downwind of the volcano (Figure 5 e–f).

Our observations capture the impact primarily of low altitude aerosol emission. However, our observations of VAIE are not limited to inter-eruptive emission. In Figure 9 aerosol and cloud properties are split according to whether or not Piton de la Fournaise was erupting (as recorded in the Smithsonian database *Siebert and Simkin*, 2002–). Aerosol is elevated all around the volcano during periods of eruption (compare Figures 9 a and b), but particularly in the downwind quadrant. Similarly, CER is lowest during periods of eruption in the downwind sector (compare Figures 9 c and d).

3.4 Distinguishing between orographic and volcanic effects

Orographic clouds form when moist air is forced upwards by high topography so that it expands and cools below its saturation point. Their form depends on relative humidity, wind speed and the height and geometry of topography. At high humidity and lower wind speeds, droplets condense above the windward slopes of a mountain, sometimes causing orographic precipitation. Wave clouds may also form in perpendicular bands downwind of high topography. At isolated, steep sided mountains high wind speeds can cause local uplifting on the upper slopes in the lee side of the mountain ('banner cloud'). As the formation of orographic cloud is controlled by wind strength and direction, its presence is expected to introduce systematic features to our rotated cloud properties.

For a tall, isolated island, orographic clouds may form (1) over high land upwind of the summit and (2) at the crests of lee waves (rotor and lenticular clouds), downwind and extending hundreds of kilometres away from the island (e.g. *Houze*, 1994). We observe elevated COD in averaged cloud property data over the islands with high topography (Kīlauea, Réunion, Fiji and to some extent Tristan da Cunha). COD is elevated immediately upwind of the islands' summit and remains high over land downwind. Any difference in COD between the windward and lee sides of the islands at greater distance is very low, suggesting that the contribution of wave clouds to the average values is small.

This is confirmed by estimating the average cloud properties for days with different tropospheric stabilities (Figure 10). Tropospheric stability was approximated by the unsaturated moist Froude number estimated from ECMWF reanalysis data: $\mathrm{Fr}^2 = \frac{\mathrm{u}^2}{\mathrm{N}^2\mathrm{h}^2}$, where u is wind speed at the height (h) of the island and N is the unsaturated moist Brunt-Väisälä frequency. N is also estimated from ECMWF temperatures at atmospheric pressures >750 mb ($\mathrm{N}^2 = \frac{g}{\theta_v}\frac{\delta\theta_v}{\delta z}$, where g = gravitational acceleration, θ_v = virtual potential temperature and z = atmospheric thickness). Where Froude number is low (< 0.1, blue on Figure 10) air will flow around a mountain, rather than over it. For Froude numbers closer to 1 (0.1–0.5, green and > 0.5 red on Figure 10), lee waves and wave clouds will form. At higher Froude numbers air flows over the island very fast and there are no stable layers. Although COD is higher at greater Froude number at Yasur and Piton de la Fournaise (Figure 10), atmospheric stability seems to have a limited effect on systematic differences between CER upwind and downwind.

Orographic cloud has smaller droplets at a higher density than marine clouds. For example, *Jiusto*'s (1967) aircraft sampling of both marine and orographic cloud upwind of Kīlauea, found that marine clouds had an average radius of 22 ± 3 μm, (droplet concentration 45 ± 22 cm^{-3}) while clouds on the flanks of Mauna Loa had an average radius of 14 ± 3 μm (droplet concentration 100 ± 50 cm^{-3}). Although the values are not directly comparable, we find a similar decrease in droplet size (seasonal averages -2 – -8 μm, see Table 2) on the windward side of Big Island Hawai'i. However, CER does not reach its minimum value until almost 100 km downwind, and remains lower than upwind values until almost 400 km from land (see Figure 3). We see no such effect in clouds downwind from Fiji (also $\sim$ 100 km across and in the path of easterly trade winds, but lower in elevation) or American Samoa, but Tristan da Cunha shows a small decrease in droplet size in data from December-February. We note that this decrease in CER downwind of Tristan da Cunha correlates well with a downwind increase in COD. At the active volcanoes (e.g. Figure 3c or k), downwind CER remains low at greater distances from the vent than COD remains elevated. CER, though influenced by orographic processes, is more strongly affected by volcanogenic aerosol at Kīlauea and Piton de la Fournaise, and regional trends in cloud properties at Yasur.

3.5 Consistency of Measurements and Sources of Uncertainty

The general trends in aerosol and cloud properties retrieved from MODIS and AATSR are consistent: both instruments show elevated AOD and suppressed CER downwind of the volcanoes but not control islands, and elevated COD over all land (Figure 8, Table 2). However, seasonal differences vary between the instruments and AATSR results generally have much higher standard errors than MODIS due to longer re-

peat time (3 days relative to 1 day), shorter period of coverage (6 relative to 10 years) and consequently smaller sample size. The absolute values for CER are greater for MODIS than AATSR retrievals, likely due to the different penetration depths of the instrument wavelengths. The wavelengths most sensitive to CER are 1.6 μm and 2.1 μm for AATSR ORAC and MODIS (Joint Atmosphere product) retrieval algorithms respectively. The shorter wavelength used by AATSR penetrates deeper into the clouds, so will sample smaller cloud droplets in a non-precipitating cloud, which typically have increasing cloud droplet size with height (*Platnick*, 2000; *Sayer et al.*, 2011).

Standard error in seasonal and multi-annual averages is greatest over land for both cloud and aerosol properties (large error bars on Figures 3 and 4). This is the result of a) fewer data points contributing to the mean (i.e. an arc of $\frac{\pi}{2}$ is shorter closer to the volcano) and b) a greater spread in the retrieval values made over land. Observations made beyond the extent of the island are therefore most robust. The higher uncertainty in retrievals made over land may also contribute to the 'anticipation' of the volcano, seen, for example, ~ 50 km upwind of Kīlauea in Figure 3 a and Yasur in Figure 3 b. Uncertainties in ECMWF wind direction will smear upwind-downwind differences radially in our analysis. Isolated topographic peaks, such as these volcanoes, introduce perturbations to the regional wind fields, resulting in local turbulence near the volcano itself and local differences from the ECMWF wind fields (spatial resolution = 1.5°) used in our analysis.

As aerosol and cloud properties are both dependent on the same meteorological processes, there is a potential for spurious correlation between AOD and cloud properties, unrelated to volcanic aerosol. For example, cyclones are associated with both increased cloud fraction (*Field and Wood*, 2007) and increased AOD due to high relative humidity and wind speeds, resulting in elevated hygroscopic growth of aerosols (e.g. *Seinfeld and Pandis*, 1998; *Twohy et al.*, 2009) as well as increased sea spray emission (e.g., *Grandey et al.*, 2011). Artefacts in satellite retrievals of AOD under broken cloudy conditions may also lead to spurious correlations between aerosol and cloud properties (*Grandey et al.*, 2013), but as we use retrievals from the full range of atmospheric conditions such effects should not have a significant impact on our results. False correlations between aerosol and cloud properties may also be introduced by analysis of satellite data over large regions containing significant variation in aerosol type, cloud regime and average synoptic conditions (*Grandey and Stier*, 2010). We limit the chance of our results being affected by spurious correlations due to spatial variations in climate by limiting measurements to regions of up to only 4 degrees across, the largest regional size recommended by *Grandey and Stier* (2010) for analysis of AIE. Only in data from the 4° surrounding Yasur do we observe a systematic regional trend in aerosol properties. There were many more cloud retrievals (cloud fraction > 0.2, Figure 7) downwind than upwind, though COD remained similar. This means that although aerosols are elevated downwind of Yasur, there is not evidence of statistically significant AIE.

4 Discussion

4.1 Observations of Volcanic Aerosol

The identification of VAIE is easiest where other sources of aerosol are low. We assume that for the islands discussed here, primary sea spray aerosol dominates aerosol populations (e.g. *Sayer et al.*, 2012; *Smirnov et al.*, 2012; *Huang et al.*, 2010). We test this assumption by examining the linear relationships between mean daily AOD and surface wind speeds within 50 km radius of the volcanoes (Figure 11). The slopes of the linear regression between AOD and binned wind speed take values ranging from 0.003–0.005 for Kīlauea, Yasur and La Réunion, respectively in Figure 11. This is within the range found by *Smirnov et al.* (2012) from examination of ship-borne sun photometer AOD measurements and near surface wind speeds (0.004–0.005). This supports the assumption that sea spray is the most important background aerosol at these volcanoes, rather than, for example, organic carbon or mineral dust from the islands.

Time series of daily AOD from MODIS data all show a large day to day variability. This is partially attributable to the amount of both sea spray and volcanogenic aerosol being heavily dependent on synoptic conditions. Although the emission of volcanic gases is independent of atmospheric conditions, the oxidising agents and reaction rates for the formation of SO_4^{2-} from SO_2 are dependent on atmospheric conditions such as supersaturation and solar irradiation levels (*Eatough et al.*, 1995). The formation of aerosol may take place in a different manner in clear and cloudy conditions, and dilution effects will also vary with wind speed and direction. The emission of volcanic gases also varies through time. While at Kīlauea, SO_2 emission is passive and accompanies long-lived flows and lava lake activity, at Yasur gas flux and composition varies more rapidly according the stage of Strombolian explosion. At Piton de la Fournaise inter-eruptive flux is low, but SO_2 emission accompanies frequent minor explosions and lava flows. There is a general correlation between net downwind aerosol at the three volcanoes and average background (inter-eruptive) SO_2 flux (e.g. Tables 1 and 2).

4.2 Volcanic aerosol and cloud interaction

The impact of volcanogenic aerosol depends on synoptic conditions and the state of any pre-existing cloud. Secondary sulphate aerosol formed from ambient reactions of volcanic SO_2 are typically <0.1 μm in diameter, and are therefore too small to act as CCN where the level of supersaturation is low (e.g. *Pierce and Adams*, 2007). Aerosol from shipping most commonly results in tracks of lower CER where

the aerosol plume is able to mix directly with an overlying cloud deck before major dispersal. Typical ship tracks form when the boundary layer is shallow (< 800 m), wind speeds are moderate, relative humidity is high and the difference in temperature between air and sea is low (*Durkee et al.*, 2000). The impact of additional CCN on orographic cloud has been less well studied, and conditions most likely to result in cloud brightening are unclear (*Muhlbauer et al.*, 2010).

All of the islands investigated here are in regions where the free atmosphere is dominated by trade winds, except Tristan da Cunha, where westerlies dominate. We expect that the measurements of cloud properties are most commonly from decks of marine stratocumulus over the oceans, with contributions from orographic cloud over land and in the islands' wakes. As our results consist of seasonal and multi-annual averages of retrievals, they contain contributions from days with a range of meteorological conditions (Mean COD and cloud top pressures for MODIS data 2002-2013 are shown in the Supplementary Figure). The mean values for COD and CER presented here therefore capture net conditions and may not bear a resemblance to the atmospheric processes on any particular day. Our measurements of time-averaged impact would be complemented by case-by-case analysis of volcanic tracks (e.g. *Gassó*, 2008) to improve our understanding of the influence of atmospheric conditions and emission characteristics on cloud properties.

4.3 Evidence for volcanic aerosol indirect effects

The anticorrelation between AOD and CER values downwind of the degassing volcanoes provides strong evidence for a first indirect effect at Kīlauea and Piton de la Fournaise. This is confirmed by the perturbation to ToA upward SW flux downwind of the active volcanoes seen in CERES data. At all the active volcanoes minimum CER is found at similar downwind distance as peak AOD in averaged retrieval data. The difference between background (upwind) CER and the minimum value found downwind is greatest at Kīlauea (up to -8 μm, decrease of 35%) and lower at Yasur and Piton de la Fournaise (up to -4 μm, decrease of 18%). This difference far exceeds the expected uncertainty in MODIS CER retrievals of 2–3.5% (*Platnick et al.*, 2003). In common with the persistent downwind elevation in AOD, CER at Kīlauea and Yasur remains lower than upwind values at least as far as 400 km downwind, while CER returns to its average upwind value within 100 km at Réunion. Droplets in 'clean' clouds upwind of the volcanoes have average droplet effective radii of 21-22 μm.

The presence of secondary AIE are harder to demonstrate. Liquid water path (LWP, kgm^{-2}) reaches its peak value within $\sim$ 50 km of the volcanic vents and is very slightly elevated downwind relative to upwind at the volcanoes (Figure 3 and 4). This could indicate an increase in cloud lifetime due to drizzle suppression (e.g. *Lohmann et al.*, 2005), but it may also be the consequence of the contribution of cooling and condensing water vapour emitted from the volcano. At Kīlauea, and to some extent Piton de la Fournaise, there were an elevated number of cloud retrievals with cloud fraction >0.2 downwind relative to upwind (Figure 7). Water vapour flux at Yasur exceeds 13×10^3 Mg/day (*Métrich et al.*, 2011). Emissions of water vapour into the atmosphere at Kīlauea and Piton de la Fournaise will be even greater due to the additional contribution of evaporated seawater where lava flows meet the sea (e.g. *Edmonds and Gerlach*, 2006; *Gouhier and Coppola*, 2011). The condensation of evaporated seawater may result in an increase in LWP content downwind that would mask any evidence of secondary AIE.

In spite of the strong correlation, our MODIS and AATSR measurements do not allow a direct measurement of the Twomey effect because retrievals of aerosol and cloud properties are mutually exclusive (i.e. aerosol properties are retrieved only where pixels are not flagged as cloud). However, the increase in average downwind ToA upward SW flux seen in CERES data for all sky conditions shows a radiative impact over a similar area to the downwind cloud and aerosol perturbations, providing additional evidence of a first indirect effect associated with volcanic aerosol.

5 Extrapolating to global volcanic aerosol indirect effects

Elevated AOD and suppressed CER are observed over a decade downwind of three persistently active volcanoes with different eruptive characteristics: Kīlauea (strong degassing), Yasur (Strombolian eruptions) and Piton de la Fournaise (minor explosions and lava flows). Top of Atmosphere Short Wave radiative flux is apparently elevated by at least 10 Wm^{-2} downwind of all three degassing volcanoes at distances $>$ 150 km, and is even higher within 100 km downwind of Kīlauea and Piton de la Fournaise. Time-averaged cloud data at three 'control' islands showed no significant suppression of CER downwind of the islands or perturbation to ToA upward SW flux exceeding $\pm$ 10 Wm^{-2}.

Our approach builds on previous studies of volcano tracks during periods of elevated activity (*Gassó*, 2008; *Yuan et al.*, 2011) by estimating average volcanic impact over 6–10 years. This is a step towards the measurement of the long-term impact of persistent volcanic activity in the present day atmosphere. In the three test cases described here, we observe some general trends that could be extrapolated to other volcanoes. High average downwind AOD is linked with high background SO_2 flux. Although daily ground-based measurements of SO_2 do not necessarily correlate with daily satellite retrievals of AOD, average background SO_2 flux at the three volcanoes is proportional to time-averaged upwind–downwind difference in AOD (Tables 1 and 2). Both the greatest upwind–downwind differences in AOD and CER and the greatest distance to minimum CER were found at Kīlauea, the volcano with the greatest SO_2 flux.

Of the 49 continuously erupting volcanoes for which *Andres and Kasgnoc* (1998) present SO_2 fluxes, only 8 are islands further than $\sim$ 50 km from the nearest land mass and together contribute $\sim$14% of the SO_2 flux in the compilation. Our observations at Kīlauea and Yasur alone capture the local impact of about half of these emissions. The remaining SO_2 flux from continuously degassing volcanoes originates on the continents (24 volcanoes) or within $\sim$ 50 km of the nearest large landmass (17 volcanoes). These 'coastal' volcanoes, including Etna, Bagana and Sakura-jima, emit almost $\sim$ 50 % of global continuous emissions (*Andres and Kasgnoc*, 1998). Observations of AIE in continental or coastal settings may be achievable using trajectory analysis of air parcels from the volcano to allow comparison of aerosol laden atmosphere to average background conditions. Our observations of VAIE at Piton de la Fournaise demonstrate that active volcanoes without a constant SO_2 flux to the atmosphere also have an impact on time-averaged local cloud properties. A complete inventory of tropospheric cloud alteration by volcanoes should therefore also include emissions associated with minor explosions.

The VAIE observed in this study is unlikely to be representative of the average present day impact of volcanoes worldwide. Importantly, the impact of additional aerosols on cloud microphysics is greater for pristine clouds than for polluted regions (e.g. *Lohmann et al.*, 2005; *Rosenfeld et al.*, 2008). The change in cloud droplet size downwind of Kīlauea, Yasur and Piton de la Fournaise is expected to be large relative to that for volcanoes that emit aerosol into heavily polluted cloud decks (e.g. Etna, Masaya). However, these observations of the most pristine parts of the Earth's present day atmosphere are likely to be the best observable analogue of pre-industrial aerosol effects.

Acknowledgements. We thank Santiago Gassó for useful discussions at the inception of this project and during manuscript preparation. SKE is funded by the UK National Environmental Research Council through the COMET/NCEO and STREVA programmes. RGG, TAM and EC are also supported by COMET/NCEO. GRAPE data are hosted by the BADC and MODIS data are hosted by NASA LAADS.

References

Ackerman, A. S., O. B. Toon, J. P. Taylor, D. W. Johnson, P. V. Hobbs, and R. J. Ferek, Effects of Aerosols on Cloud Albedo: Evaluation of Twomey's Parameterization of Cloud Susceptibility Using Measurements of Ship Tracks., *Journal of Atmospheric Sciences*, *57*, 2684–2695, 2000.

Ackerman, A. S., M. P. Kirkpatrick, D. E. Stevens, and O. B. Toon, The impact of humidity above stratiform clouds on indirect aerosol climate forcing, *Nature*, *432*(7020), 1014–1017, 2004.

Ackerman, S., R. Holz, R. Frey, E. Eloranta, B. Maddux, and M. McGill, Cloud detection with MODIS. Part II: validation, *Journal of Atmospheric and Oceanic Technology*, *25*(7), 1073–1086, 2008.

Albrecht, B., Aerosols, cloud microphysics, and fractional cloudiness., *Science (New York, NY)*, *245*(4923), 1227, 1989.

Allen, A., C. Oppenheimer, M. Ferm, P. Baxter, L. Horrocks, B. Galle, A. McGonigle, and H. Duffell, Primary sulfate aerosol and associated emissions from Masaya Volcano, Nicaragua, *Journal of Geophysical Research*, *107*(D23), 4682, 2002.

Andreae, M. O., et al., Aerosols before pollution, *Science(Washington)*, *315*(5808), 50–51, 2007.

Andres, R., and A. Kasgnoc, A time-averaged inventory of subaerial volcanic sulfur emissions, *Journal of Geophysical Research*, *103*(D19), 25,251–25, 1998.

Bani, P., and M. Lardy, Sulphur dioxide emission rates from Yasur volcano, Vanuatu archipelago, *Geophysical Research Letters*, *34*, L20309, 2007.

Bani, P., C. Oppenheimer, P. Allard, H. Shinohara, V. Tsanev, S. Carn, M. Lardy, and E. Garaebiti, First estimate of volcanic SO_2 budget for Vanuatu island arc, *Journal of Volcanology and Geothermal Research*, *211*, 36–46, 2012.

Bhugwant, C., B. Siéja, M. Bessafi, T. Staudacher, and J. Ecormier, Atmospheric sulfur dioxide measurements during the 2005 and 2007 eruptions of the Piton de La Fournaise volcano: Implications for human health and environmental changes, *Journal of Volcanology and Geothermal Research*, *184*, 208–224, 2009.

Brenguier, J., H. Pawlowska, and L. Schüller, Cloud microphysical and radiative properties for parameterization and satellite monitoring of the indirect effect of aerosol on climate, *Journal of Geophysical Research*, *108*(D15), 8632, 2003.

Campmany, E., R. G. Grainger, S. M. Dean, and A. M. Sayer, Automatic detection of ship tracks in ATSR-2 satellite imagery, *Atmospheric Chemistry & Physics*, *9*, 1899–1905, 2009.

Carslaw, K. S., L. A. Lee, C. L. Reddington, K. J. Pringle, A. Rap, P. M. Forster, G. W. Mann, D. V. Spracklen, M. T. Woodhouse, L. Regayre, and J. R. Pierce, Large contribution of natural aerosols to uncertainty in indirect forcing, *Nature*, *503*, 67–71, 2013.

Chen, Y.-C., M. W. Christensen, L. Xue, A. Sorooshian, G. L. Stephens, R. M. Rasmussen, and J. H. Seinfeld, Occurrence of lower cloud albedo in ship tracks, *Atmospheric Chemistry and Physics*, *12*(17), 8223–8235, 2012.

Christensen, M. W., and G. L. Stephens, Microphysical and macrophysical responses of marine stratocumulus polluted by underlying ships: Evidence of cloud deepening, *Journal of Geophysical Research: Atmospheres (1984–2012)*, *116*(D3), 2011.

Coppola, D., D. Piscopo, T. Staudacher, and C. Cigolini, Lava discharge rate and effusive pattern at Piton de la Fournaise from MODIS data, *Journal of Volcanology and Geothermal Research*, *184*(1-2), 174–192, 2009.

Dee, D. P., S. M. Uppala, A. J. Simmons, P. Berrisford, P. Poli, S. Kobayashi, U. Andrae, M. A. Balmaseda, G. Balsamo, P. Bauer, P. Bechtold, A. C. M. Beljaars, L. van de Berg, J. Bidlot, N. Bormann, C. Delsol, R. Dragani, M. Fuentes, A. J. Geer, L. Haimberger, S. B. Healy, H. Hersbach, E. V. Hólm, L. Isaksen, P. Kållberg, M. Köhler, M. Matricardi, A. P. McNally, B. M. Monge-Sanz, J.-J. Morcrette, B.-K. Park, C. Peubey, P. de Rosnay, C. Tavolato, J.-N. Thépaut, and F. Vitart, The ERA-Interim reanalysis: configuration and performance of the data assimilation system, *Quarterly Journal of the Royal Meteorological So-*

ciety, *137*(656), 553–597, 2011.

Dentener, F., S. Kinne, T. Bond, O. Boucher, J. Cofala, S. Generoso, P. Ginoux, S. Gong, J. Hoelzemann, A. Ito, et al., Emissions of primary aerosol and precursor gases in the years 2000 and 1750 prescribed data-sets for aerocom, *Atmospheric Chemistry and Physics*, *6*(12), 4321–4344, 2006.

Di Muro, A., A. Aiuppa, M. Burton, N. Metrich, P. Allard, T. Fougeroux, G. Giudice, and R. Guida, Intra-eruptive gas emissions and shallow magma storage after the 2007 summit caldera collapse of Piton de la Fournaise, Reunion island., in *EGU General Assembly Conference Abstracts*, *EGU General Assembly Conference Abstracts*, vol. 14, edited by A. Abbasi and N. Giesen, p. 2761, 2012.

Durkee, P. A., R. E. Chartier, A. Brown, E. J. Trehubenko, S. D. Rogerson, C. Skupniewicz, K. E. Nielsen, S. Platnick, and M. D. King, Composite Ship Track Characteristics., *Journal of Atmospheric Sciences*, *57*, 2542–2553, 2000.

Eatough, D. J., F. M. Caka, and R. J. Farber, The conversion of SO_2 to sulfate in the atmosphere, *Israel Journal of Chemistry*, *34*, 301–314, 1995.

Edmonds, M., and T. Gerlach, The airborne lava–seawater interaction plume at Kīlauea Volcano, Hawaii, *Earth and Planetary Science Letters*, *244*(1), 83–96, 2006.

Elias, T., and A. J. Sutton, Sulfur dioxide emission rates from Kilauea Volcano, Hawai'i, 2007–2010, *U.S. Geological Survey Open-File Report*, *1107*, 25p, 2012.

Field, P. R., and R. Wood, Precipitation and Cloud Structure in Midlatitude Cyclones, *Journal of Climate*, *20*, 233, 2007.

Garofalo, K., T. Staudacher, V. Ferrazzini, P. Kowalski, P. Boissier, A. Dupont, A. Peltier, B. Villemant, and G. Boudon, Eruptive so2-plume measurements at piton de la fournaise (ile de la réunion) by stationary novac scanning max-doas instruments, in *EGU General Assembly Conference Abstracts*, vol. 11, p. 12113, 2009.

Gassó, S., Satellite observations of the impact of weak volcanic activity on marine clouds, *Journal of Geophysical Research (Atmospheres)*, *113*(D12), D14S19, 2008.

Geier, E., R. Green, D. Kratz, P. Minnis, W. Miller, S. Nolan, and C. Franklin, Ceres data management system: Single satellite footprint toa/surface fluxes and clouds (ssf) collection document, release 2, version 1, 212 pp. and appendixes, nasa langley res. cent., hampton, va, *Radiat. and Aerosol Branch, Atmos. Sci. Res., NASA Langley Res. Cent., Hampton, Va.(Available online at http://asd-www. larc. nasa. gov/ceres/collect_guide/SSF_CG. pdf)*, 2003.

Gouhier, M., and D. Coppola, Satellite-based evidence for a large hydrothermal system at Piton de la Fournaise volcano (Reunion Island), *Geophysical Research Letters*, *38*, L02302, 2011.

Graf, H., B. Langmann, and J. Feichter, The contribution of Earth degassing to the atmospheric sulfur budget, *Chemical Geology*, *147*(1-2), 131–145, 1998.

Grandey, B. S., and P. Stier, A critical look at spatial scale choices in satellite-based aerosol indirect effect studies, *Atmospheric Chemistry & Physics*, *10*, 15,417–15,440, 2010.

Grandey, B. S., P. Stier, T. M. Wagner, R. G. Grainger, and K. I. Hodges, The effect of extratropical cyclones on satellite-retrieved aerosol properties over ocean, *Geophysical Research Letters*, *38*, L13805, 2011.

Grandey, B. S., P. Stier, and T. M. Wagner, Investigating relationships between aerosol optical depth and cloud fraction using satellite, aerosol reanalysis and general circulation model data, *Atmospheric Chemistry & Physics*, *13*, 3177–3184, 2013.

Halmer, M., H. Schmincke, and H. Graf, The annual volcanic gas input into the atmosphere, in particular into the stratosphere: a global data set for the past 100 years, *Journal of Volcanology and Geothermal Research*, *115*(3), 511–528, 2002.

Hansen, J., M. Sato, R. Ruedy, et al., Radiative forcing and climate response, *Journal of Geophysical Research*, *102*, 6831–6864, 1997.

Houze, R. A. J., *Cloud dynamics*, vol. 53, Access Online via Elsevier, 1994.

Huang, H., G. E. Thomas, and R. G. Grainger, Relationship between wind speed and aerosol optical depth over remote ocean, *Atmospheric Chemistry & Physics*, *10*, 5943–5950, 2010.

Jiusto, J., Aerosol and cloud microphysics measurements in Hawai'i, *Tellus*, *19*(3), 359–368, 1967.

Khokhar, M., C. Frankenberg, M. van Roozendael, S. Beirle, S. Kühl, A. Richter, U. Platt, and T. Wagner, Satellite observations of atmospheric SO_2 from volcanic eruptions during the time-period of 1996–2002, *Advances in Space Research*, *36*, 879–887, 2005.

Lee, L., K. Pringle, C. Reddington, G. Mann, P. Stier, D. Spracklen, J. Pierce, and K. Carslaw, The magnitude and causes of uncertainty in global model simulations of cloud condensation nuclei, *Atmospheric Chemistry and Physics*, *13*, 8879–8914, 2013.

Levy, R. C., S. Mattoo, L. A. Munchak, L. A. Remer, A. M. Sayer, F. Patadia, and N. C. Hsu, The Collection 6 MODIS aerosol products over land and ocean, *Atmospheric Measurement Techniques*, *6*(11), 2989–3034, 2013.

Lohmann, U., J. Feichter, et al., Global indirect aerosol effects: a review, *Atmospheric Chemistry and Physics*, *5*(3), 715–737, 2005.

Martin, G., M. Ringer, V. Pope, A. Jones, C. Dearden, and T. Hinton, The physical properties of the atmosphere in the new hadley centre global environmental model (hadgem1). part i: Model description and global climatology, *Journal of Climate*, *19*(7), 1274–1301, 2006.

Martin, R., T. Mather, D. Pyle, M. Power, A. Allen, A. Aiuppa, C. Horwell, and E. Ward, Composition-resolved size distributions of volcanic aerosols in the Mt. Etna plumes, *Journal of Geophysical Research*, *113*(D17), D17,211, 2008.

Mather, T., J. McCabe, V. Rai, M. Thiemens, D. Pyle, et al., Oxygen and Sulfur isotopic composition of volcanic sulfate aerosol at the point of emission, *Journal of Geophysical Research*, *111*(D18), D18,205, 2006.

Mather, T., M. Witt, D. Pyle, B. Quayle, A. Aiuppa, E. Bagnato, R. Martin, K. Sims, M. Edmonds, A. Sutton, et al., Halogens and trace metal emissions from the ongoing 2008 summit eruption of Kīlauea volcano, Hawai'i, *Geochimica et Cosmochimica Acta*, 2012.

Mather, T. A., D. M. Pyle, and C. Oppenheimer, Tropospheric volcanic aerosol, *Geophysical Monograph Series*, *139*, 189–212, 2003.

Mather, T. A., V. I. Tsanev, D. M. Pyle, A. J. S. McGonigle, C. Oppenheimer, and A. G. Allen, Characterization and evolution of tropospheric plumes from Lascar and Villarrica volcanoes, Chile, *Journal of Geophysical Research (Atmospheres)*, *109*(D18), D21303, 2004.

Métrich, N., P. Allard, A. Aiuppa, P. Bani, A. Bertagnini, H. Shinohara, F. Parello, A. Di Muro, E. Garaebiti, O. Belhadj, et al., Magma and volatile supply to post-collapse volcanism and block resurgence in Siwi Caldera (Tanna Island, Vanuatu Arc), *Journal of Petrology*, *52*(6), 1077–1105, 2011.

Muhlbauer, A., T. Hashino, L. Xue, A. Teller, U. Lohmann, R. M. Rasmussen, I. Geresdi, and Z. Pan, Intercomparison of aerosol-cloud-precipitation interactions in stratiform orographic mixed-phase clouds, *Atmospheric Chemistry & Physics*, *10*, 8173–8196, 2010.

Oppenheimer, C., B. Scaillet, and R. S. Martin, Sulfur degassing from volcanoes: source conditions, surveillance, plume chemistry and earth system impacts, *Reviews in Mineralogy and Geochemistry*, *73*(1), 363–421, 2011.

Peltier, A., P. Bachèlery, and T. Staudacher, Magma transport and storage at Piton de La Fournaise (La Réunion) between 1972 and 2007: A review of geophysical and geochemical data, *Journal of Volcanology and Geothermal Research*, *184*(1), 93–108, 2009.

Peters, K., J. Quaas, and H. Graßl, A search for large-scale effects of ship emissions on clouds and radiation in satellite data, *Journal of Geophysical Research: Atmospheres*, *116*(D24), n/a–n/a, 2011.

Pierce, J. R., and P. J. Adams, Efficiency of cloud condensation nuclei formation from ultrafine particles, *Atmospheric Chemistry and Physics*, *7(5)*, 1376–1379, 2007.

Platnick, S., Vertical photon transport in cloud remote sensing problems, *Journal of Geophysical Research: Atmospheres*, *105*(D18), 22,919–22,935, 2000.

Platnick, S., M. D. King, S. A. Ackerman, W. P. Menzel, B. A. Baum, J. C. Riédi, and R. A. Frey, The MODIS cloud products: Algorithms and examples from Terra, *Geoscience and Remote Sensing, IEEE Transactions on*, *41*(2), 459–473, 2003.

Porter, J. N., K. A. Horton, P. J. Mouginis-Mark, B. Lienert, S. K. Sharma, E. Lau, A. J. Sutton, T. Elias, and C. Oppenheimer, Sun photometer and lidar measurements of the plume from the Hawaii Kilauea Volcano Pu'u O'o vent: Aerosol flux and SO_2 lifetime, *Geophysical Research Letters*, *29*, 1783, 2002.

Poulsen, C., R. Siddans, G. Thomas, A. Sayer, R. Grainger, E. Campmany, S. Dean, C. Arnold, and P. Watts, Cloud retrievals from satellite data using optimal estimation: Evaluation and application to ATSR, *Atmospheric Measurement Techniques*, *5*, 1889–1910, 2012.

Quaas, J., B. Stevens, P. Stier, and U. Lohmann, Interpreting the cloud cover-aerosol optical depth relationship found in satellite data using a general circulation model, *Atmospheric Chemistry and Physics*, *10*, 6129–6135, 2011.

Remer, L. A., Y. Kaufman, D. Tanré, S. Mattoo, D. Chu, J. Martins, R.-R. Li, C. Ichoku, R. Levy, R. Kleidman, et al., The MODIS aerosol algorithm, products, and validation, *Journal of the Atmospheric Sciences*, *62*(4), 947–973, 2005.

Robock, A., The climatic aftermath, *Science*, *295*(5558), 1242–1244, 2002.

Rosenfeld, D., U. Lohmann, G. Raga, C. O'Dowd, M. Kulmala, S. Fuzzi, A. Reissell, and M. Andreae, Flood or drought: How do aerosols affect precipitation?, *Science*, *321*(5894), 1309–1313, 2008.

Rosenfeld, D., S. Sherwood, R. Wood, and L. Donner, Climate Effects of Aerosol-Cloud Interactions, *science*, *343*, 379–380, 2014.

Sassen, K., Evidence for liquid-phase cirrus cloud formation from volcanic aerosols: Climatic implications, *Science*, *257*(5069), pp. 516–519, 1992.

Sayer, A., G. Thomas, and R. Grainger, A sea surface reflectance model for (A)ATSR, and application to aerosol retrievals, *Atmos. Meas. Tech*, *3*(4), 813–838, 2010.

Sayer, A., C. Poulsen, C. Arnold, E. Campmany, S. Dean, G. Ewen, R. Grainger, B. Lawrence, R. Siddans, G. Thomas, and P. Watts, Global retrieval of ATSR cloud parameters and evaluation (GRAPE): dataset assessment, *Atmospheric Chemistry and Physics*, *11*, 3913–3936, 2011.

Sayer, A., A. Smirnov, N. Hsu, and B. Holben, A pure marine aerosol model, for use in remote sensing applications, *Journal of Geophysical Research: Atmospheres*, *117*(D5), 2012.

Schmidt, A., K. S. Carslaw, G. W. Mann, M. Wilson, T. J. Breider, S. J. Pickering, and T. Thordarson, The impact of the 1783-1784 AD Laki eruption on global aerosol formation processes and cloud condensation nuclei, *Atmospheric Chemistry & Physics*, *10*, 6025–6041, 2010.

Schmidt, A., K. S. Carslaw, G. W. Mann, A. Rap, K. J. Pringle, D. V. Spracklen, M. Wilson, and P. M. Forster, Importance of tropospheric volcanic aerosol for indirect radiative forcing of climate, *Atmospheric Chemistry and Physics*, *12*(16), 7321–7339, 2012.

Seinfeld, J. H., and S. N. Pandis, *Atmospheric Chemistry and Physics, 1326 pp*, John Wiley, Hoboken, NJ, 1998.

Siebert, L., and T. Simkin, Volcanoes of the World: an Illustrated Catalog of Holocene Volcanoes and their Eruptions, *Smithsonian Institution, Global Volcanism Program Digital Information Series*, *GVP-3*, 2002–.

Siebert, L., T. Simkin, and P. Kimberly, Volcanoes of the World, 3rd Ed., *Berkley: Univeristy of California Press*, 2010.

Smirnov, A., A. M. Sayer, B. N. Holben, N. C. Hsu, S. M. Sakerin, A. Macke, N. B. Nelson, Y. Courcoux, T. J. Smyth, P. Croot, P. K. Quinn, J. Sciare, S. K. Gulev, S. Piketh, R. Losno, S. Kinne, and V. F. Radionov, Effect of wind speed on aerosol optical depth over remote oceans, based on data from the maritime aerosol network, *Atmospheric Measurement Techniques*, *5*, 377–388, 2012.

Stevens, B., and G. Feingold, Untangling aerosol effects on clouds and precipitation in a buffered system, *Nature*, (461), 607–613, 2010.

Thomas, G., C. Poulsen, A. Sayer, S. Marsh, S. Dean, E. Carboni, R. Siddans, R. Grainger, and B. Lawrence, The GRAPE aerosol retrieval algorithm, *Atmospheric Measurement Techniques*, *2*(2), 679–701, 2009.

Tulet, P., and N. Villeneuve, Large scale modeling of the transport, chemical transformation and mass budget of the sulfur emitted during the April 2007 eruption of Piton de la Fournaise, *Atmospheric Chemistry and Physics*, *11*(9), 4533–4546, 2011.

Twohy, C. H., J. A. Coakley, and W. R. Tahnk, Effect of changes in relative humidity on aerosol scattering near clouds, *Journal of Geophysical Research: Atmospheres*, *114*(D5), n/a–n/a, 2009.

Twomey, S., The influence of pollution on the shortwave albedo of clouds, *Journal of the atmospheric sciences*, *34*(7), 1149–1152, 1977.

Yuan, T., L. A. Remer, and H. Yu, Microphysical, macrophysical and radiative signatures of volcanic aerosols in trade wind cumulus observed by the A-Train, *Atmospheric Chemistry and Physics*, *11*(14), 7119–7132, 2011.

Table 1. Location, physical properties, degassing flux and eruptive character for volcanoes and 'control' islands discussed in this study. [a]

Volcano/Island	Latitude (°)	Longitude (°)	Maximum diameter of island (km)	Emission (Summit) height (m)	'Background' SO_2 flux (Mg/day)	Activity 2002-2008
Volcanoes						
Kīlauea	19.42	-155.29	130	1222 (4170)	1800 (2002–2007)[1]	Effusive lava flows, lava lake
Yasur	-19.53	169.44	40	361	633 (2004–2008)[2]	Strombolian
Piton de la Fournaise	-21.23	55.71	70	2632	Inter-eruptive flux is very low[3]	Minor explosions and basaltic flows[4]
'Control Islands'						
Fiji	-17.63	178.02	140	1324	-	-
Ofu-olosega	-14.18	169.62	9	639	-	-
Tristan da Cuhna	-37.09	-12.28	12	2060	-	-

[a] 'SO_2 flux' refers to time-averaged values of emission not associated with explosions as found from measurements presented by: [1] *Elias and Sutton* (2012), [2] *Bani et al.* (2012) and [3] *Coppola et al.* (2009); *Garofalo et al.* (2009); *Di Muro et al.* (2012). [4] Eruptions at Piton de la Fournaise occurred during: 10.2010–12.2010, 11.2009–01.2010, 09.2008–02.2009, 07.2006–05.2007, 02.2005, 05.2004–10.2004, 05.2003–01.2004 and 11.2002–12.2002, *Siebert et al.* (2010)

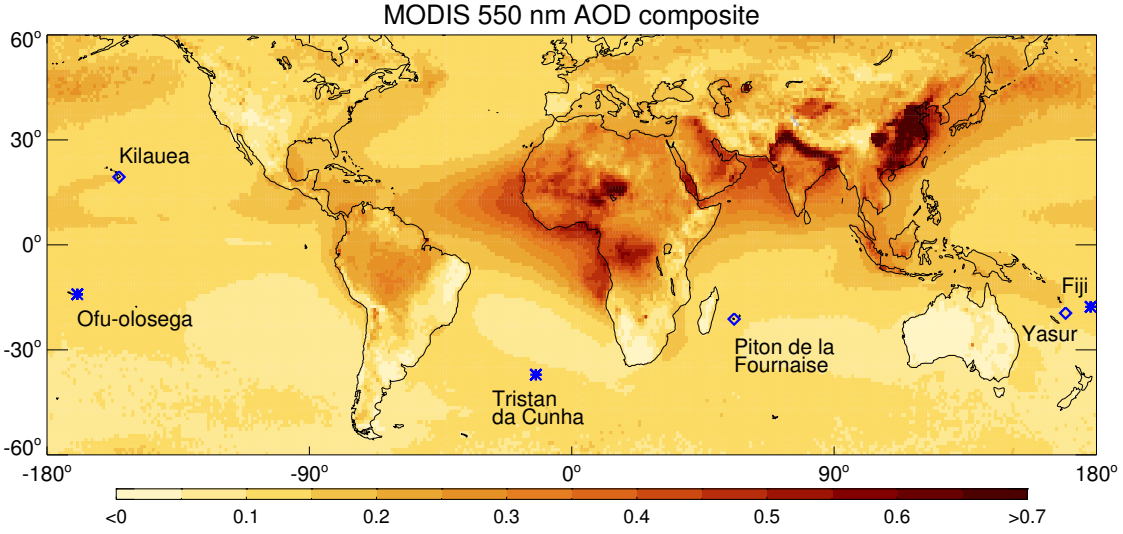

Fig. 1. a) The multiannual mean (2002–2013) of Collection 6 MODIS Aqua AOD at 550nm (merged dataset). Grey indicates that there are no data. Volcano locations are indicated by blue diamonds, 'control' islands by blue crosses.

Table 2. Average difference in upwind and downwind cloud and aerosol properties for MODIS (Aqua) and AATSR retrievals for volcanoes discussed in this study. Uncertainties are the square root of the sum of squares of the standard errors of upwind and downwind values. [a]

Volcano			Δ AOD [1]	Δ COD [2]	Δ CER (μm)[1]	peak distance (km) [3]
Piton de la Fournaise	MODIS	DJF	0.08 ± 0.03	2 ± 1	-8 ± 1	∼ 25
		MAM	0.03 ± 0.03	3 ± 1	-3 ± 1	∼ 30
		JJA	0.03 ± 0.02	2 ± 1	-3 ± 1	∼ 50
		SON	0.04 ± 0.02	< 1	-4 ± 1	∼ 40
	AATSR	DJF	0.02 ± 0.02	< 1	-4 ± 2	∼ 40
		MAM	0.03 ± 0.02	-2 ± 4	-3 ± 2	∼ 15
		JJA	0.03 ± 0.02	< 1	-2 ± 2	∼ 25
		SON	0.01 ± 0.02	< 1	-4 ± 2	-
Yasur	MODIS	DJF	0.06 ± 0.01	< 1	-4 ± 1	∼ 40
		MAM	0.03 ± 0.01	2 ± 2	-3 ± 1	∼ 25
		JJA	0.04 ± 0.01	5 ± 2	-4 ± 1	∼ 35
		SON	0.05 ± 0.01	3 ± 2	-3 ± 1	∼ 40
	AATSR	DJF	0.03 ± 0.02	< 1	< 1	-
		MAM	0.02 ± 0.02	2 ± 3	-4 ± 2	∼ 40
		JJA	0.02 ± 0.02	5 ± 3	< 1	-
		SON	0.03 ± 0.02	2 ± 3	-2 ± 2	∼ 40
Kīlauea	MODIS	DJF	0.06 ± 0.01	2 ± 1	-6 ± 1	∼ 90
		MAM	0.11 ± 0.02	4 ± 1	-6 ± 1	∼ 100
		JJA	0.14 ± 0.02	4 ± 1	-8 ± 1	∼ 70
		SON	0.05 ± 0.02	2 ± 1	-8 ± 1	∼ 90
	AATSR	DJF	0.07 ± 0.03	4 ± 2	-2 ± 1	∼ 100
		MAM	0.08 ± 0.03	5 ± 3	-4 ± 3	∼ 90
		JJA	0.08 ± 0.02	5 ± 3	-5 ± 3	∼ 90
		SON	0.06 ± 0.03	2 ± 2	-2 ± 2	∼ 90
Tristan	MODIS	DJF	-0.02 ± 0.02	2 ± 1	-2 ± 1	∼ 20
		MAM	0.01 ± 0.02	3 ± 1	-1 ± 1	∼ 20
		JJA	-0.01 ± 0.02	3 ± 1	-2 ± 1	∼ 20
		SON	0.03 ± 0.02	2 ± 1	-1 ± 1	∼ 20
	AATSR	DJF	-0.01 ± 0.03	1 ± 2	-2 ± 2	-
		MAM	-0.01 ± 0.05	-	-	-
		JJA	0.01 ± 0.06	-2 ± 2	0 ± 1	-
		SON	-0.03 ± 0.03	<1	0 ± 1	-
Ofu-olosega	MODIS	DJF	-0.03 ± 0.02	1 ± 2	0 ± 1	-
		MAM	-0.02 ± 0.02	3 ± 2	-1 ± 1	-
		JJA	-0.01 ± 0.02	0 ± 2	1 ± 1	-
		SON	-0.01 ± 0.02	1 ± 2	0 ± 1	-
	AATSR	DJF	0.02 ± 0.03	-3 ± 4	-1 ± 4	-
		MAM	0.01 ± 0.02	2 ± 6	1 ± 4	-
		JJA	0.00 ± 0.02	0 ± 8	0 ± 4	-
		SON	0.01 ± 0.02	-2 ± 6	-1 ± 4	-
Fiji	MODIS	DJF	0.04 ± 0.06	-1 ± 3	0 ± 3	-
		MAM	-	-	-	-
		JJA	0.04 ± 0.06	0 ± 4	0 ± 1	-
		SON	0.04 ± 0.06	1 ± 5	0 ± 1	-
	AATSR	DJF	-0.03 ± 0.04	-6 ± 6	1 ± 4	-
		MAM	-	-	-	-
		JJA	0.06 ± 0.05	1 ± 6	3 ± 6	-
		SON	0.04 ± 0.05	3 ± 6	4 ± 6	-

[a]Cloud top pressures are between 860 and 440 mb. [1] Difference between average upwind value (-400 to 0 km) and highest (AOD) or lowest (CER) downwind value., [2] Difference between average upwind and downwind values, [3] 'peak distance' refers to the approximate distance of peak AOD downwind from the volcanic vent.

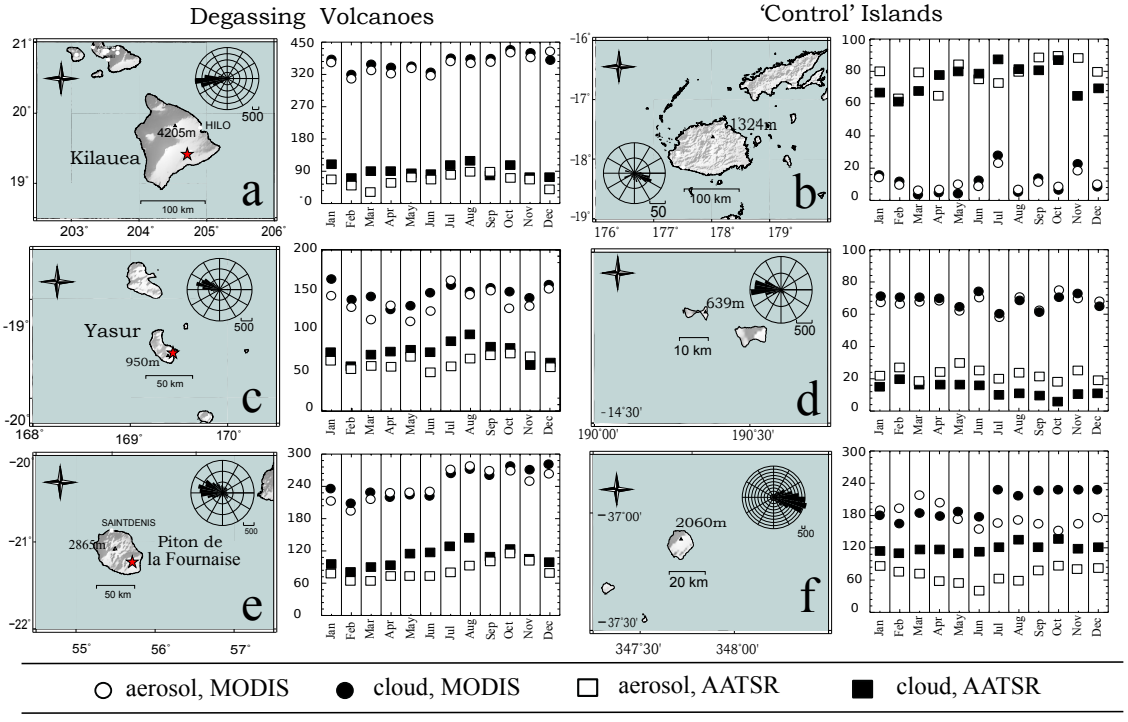

Fig. 2. a–f show dimensions, topography and seasonal distribution of data sampling for each volcano and control island in the study. Wind roses show daily ECMWF wind directions, black bars indicate the directions towards which the wind was blowing. Locations of degassing vents are marked by red stars. Bar charts show the number of retrievals used in this study for each month of the year, Squares represent number of ENVISAT retrievals, circles, MODIS. Filled shapes are cloud and outlines are aerosol.

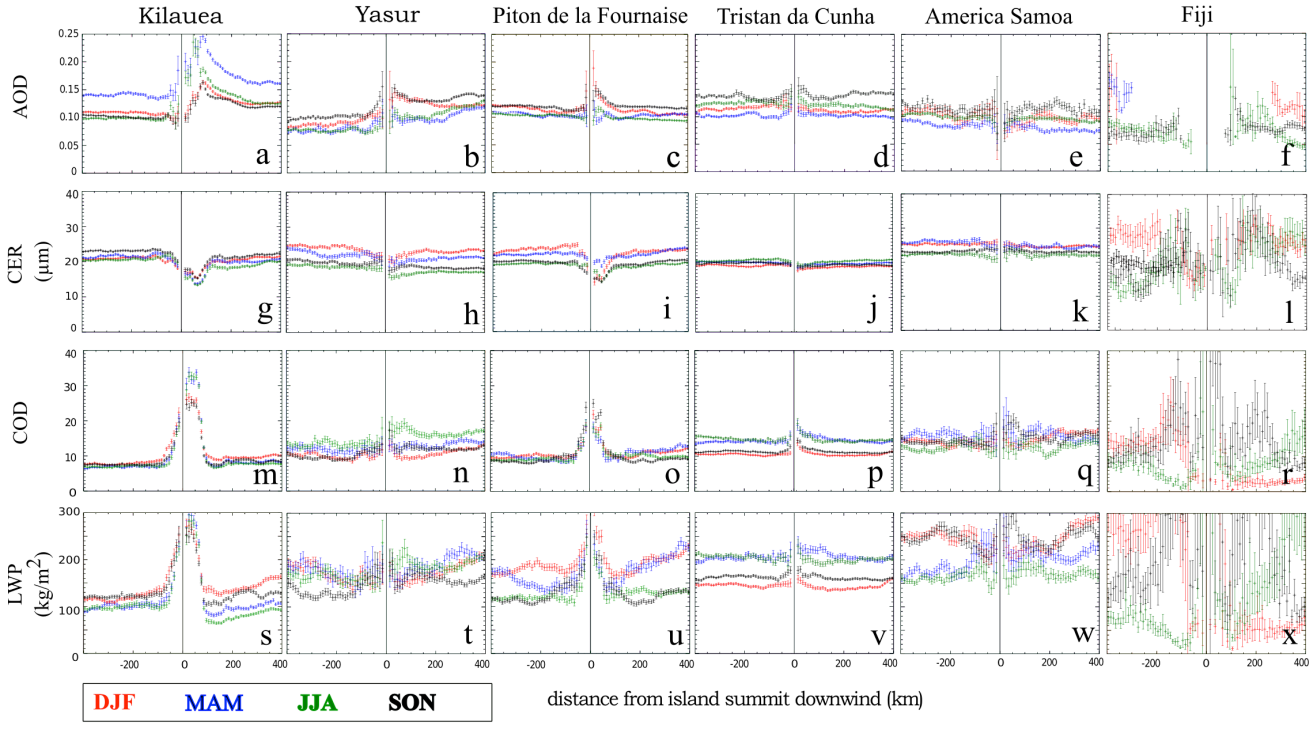

Fig. 3. Profiles of average aerosol and cloud properties upwind and downwind of the degassing volcano : Kīlauea, Hawai'i; Yasur, Vanuatu and Piton de la Fournaise, Réunion and at 'control' islands: Tristan da Cunha, South Atlantic; American Samoa, West Pacific and Fiji, West Pacific. Profile values are the average of arcs of $\frac{\pi}{2}$ at equal distance upwind and downwind from the volcano vent for MODIS Aqua data from between 2002 and 2013. Separate profiles for different time of year are shown in different colours: December–February in red, March–May in blue, June–August in green and September–November in black. Error bars show one standard error for this average and are generally larger for low sample sizes. Positive values on the x-axis are downwind, negative upwind. The maximum diameter of the islands are indicated on the parameter plots as black dashed lines.

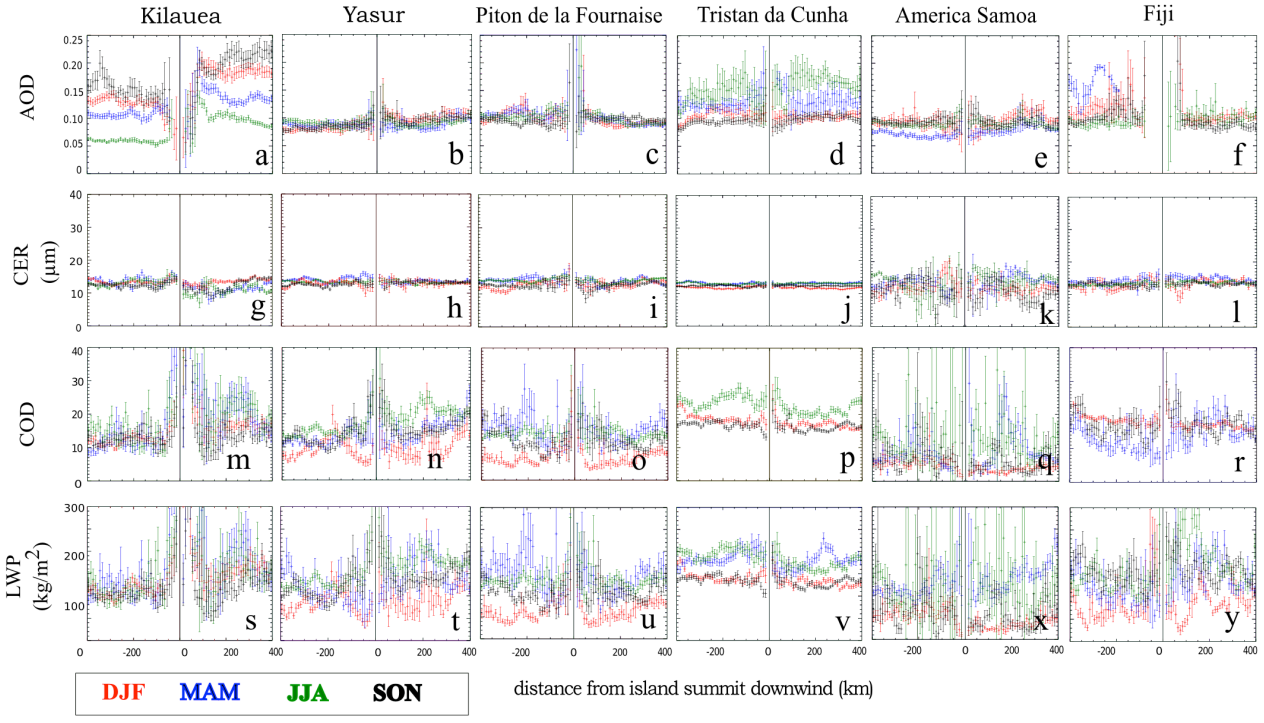

Fig. 4. Profiles of average aerosol and cloud properties upwind and downwind of the degassing volcano : Kīlauea, Hawai'i; Yasur, Vanuatu and Piton de la Fournaise, Réunion and at 'control' islands: Tristan da Cunha, South Atlantic; American Samoa, West Pacific and Fiji, West Pacific. Profile values are the average of arcs of $\frac{\pi}{2}$ at equal distance upwind and downwind from the volcano vent for AATSR between 2002 and 2008. Separate profiles for different time of year are shown in different colours: December–February in red, March–May in blue, June–August in green and September–November in black. Error bars show one standard error for this average and are generally larger for low sample sizes. Positive values on the x-axis are downwind, negative upwind. The maximum diameter of the islands are indicated on the parameter plots as black dashed lines.

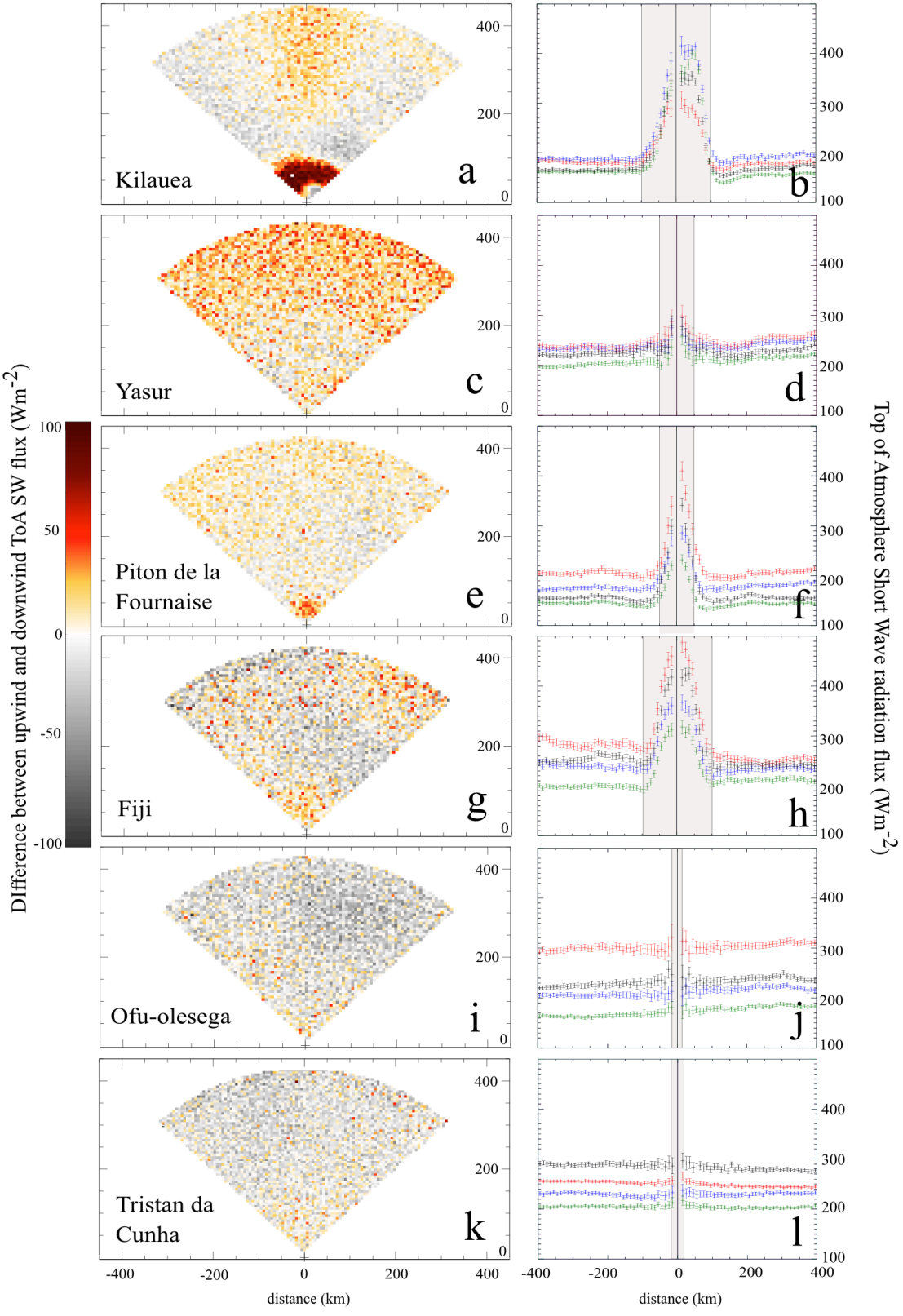

Fig. 5. Scatterplots showing the difference between upwind and downwind Top of Atmosphere Short-Wave flux (a, ,c, e, g, i, k) for volcanoes and 'controls'. Positive values indicate higher upward SW flux downwind of the volcano. Profiles (b, d, f, h, j, l) indicate seasonal average SW fluxes for arcs of $\frac{\pi}{2}$ at equal distance upwind and downwind from the volcano or island. December–February is red, March–May is blue, June–August is green and September–November is black.

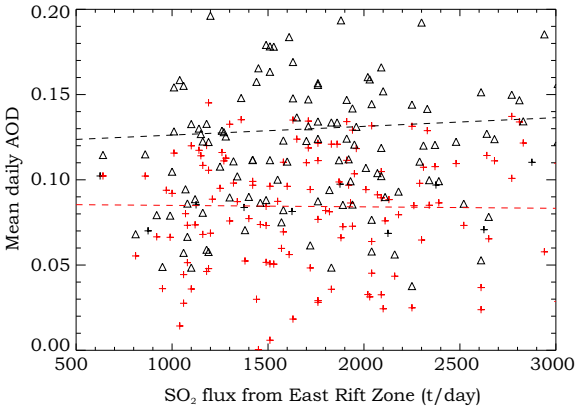

Fig. 6. Comparison of SO_2 flux from East Rift as reported by *Elias and Sutton* (2012), with AOD (550 nm) measurements from MODIS Aqua on the same day. The lack of relationship between ground and satellite-based measurements may be due to several factors including dilution effects and differences in measurement times. Black triangles show MODIS AOD retrievals and the black dashed line indicates linear regression line. The red crosses show AOD values after de-trending for a linear relationship with wind-speed, as demonstrated in Figure 11. The red dashed line shows corrected linear regression.

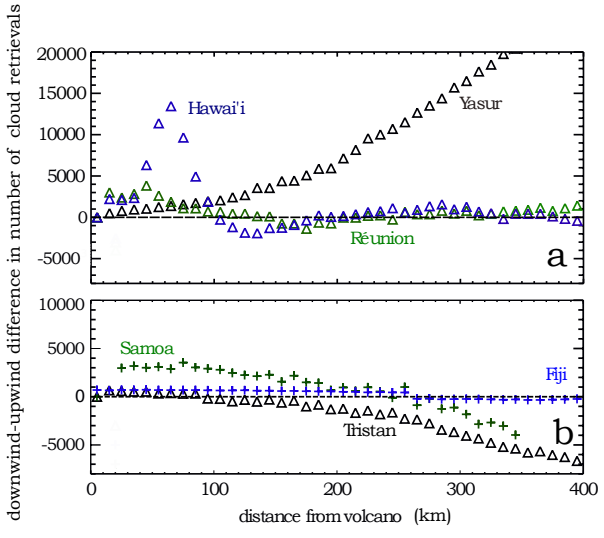

Fig. 7. Plots of the difference between numbers of cloud retrievals (cloud fraction > 0.2) downwind and upwind of volcanic vents (a) and island summits (b) from MODIS (Aqua), 2002–2008. At Hawai'i, and to some extent Réunion, there is a notable increase in the number of cloud retrievals made downwind relative to upwind within 100 km of the island.

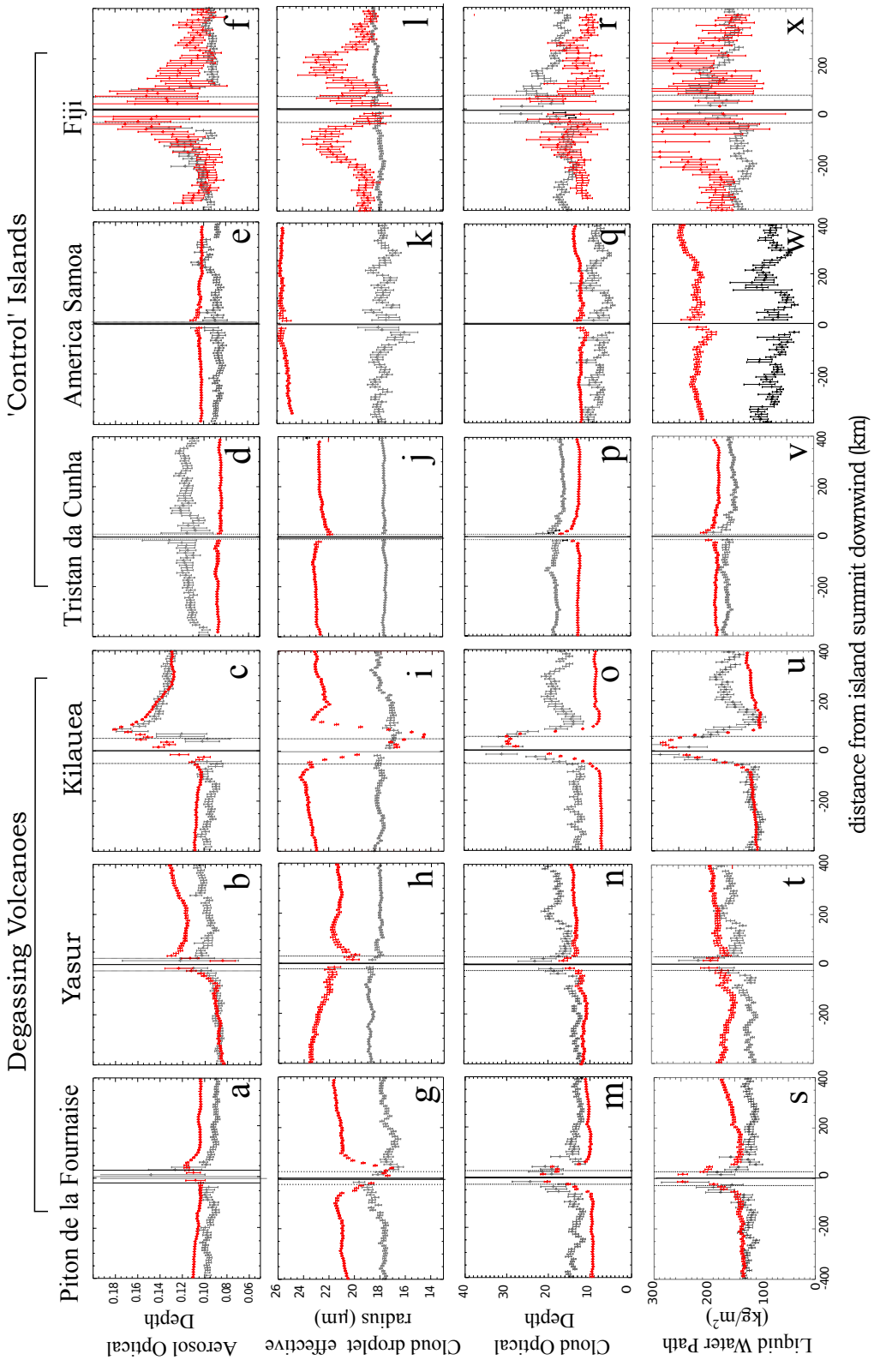

Fig. 8. Comparison of multi-annual averages for AATSR and MODIS data, presented as in Figures 3 and 4.

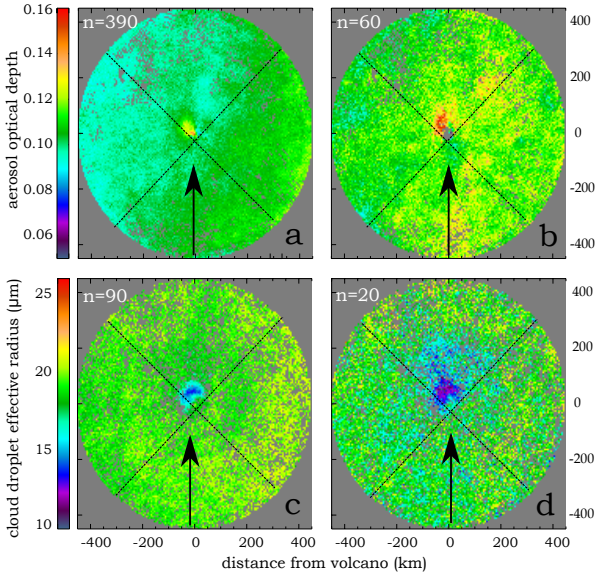

Fig. 9. Scatterplots show the average of rotated MODIS Aqua AOD (a & b) and CER (c & d) at Piton de la Fournaise during inter-eruptive (a & c) and eruptive (b & d) periods, 2002–2008. Cloud top pressures are 860–440 mb. The volcano summit is at (0,0) and arrows indicate wind direction. Downwind is the upper quadrant in each case. 'n' values refer to the average sample size in each image. Only data where sample sizes exceed 15 and relative standard deviations are less than 10% are shown.

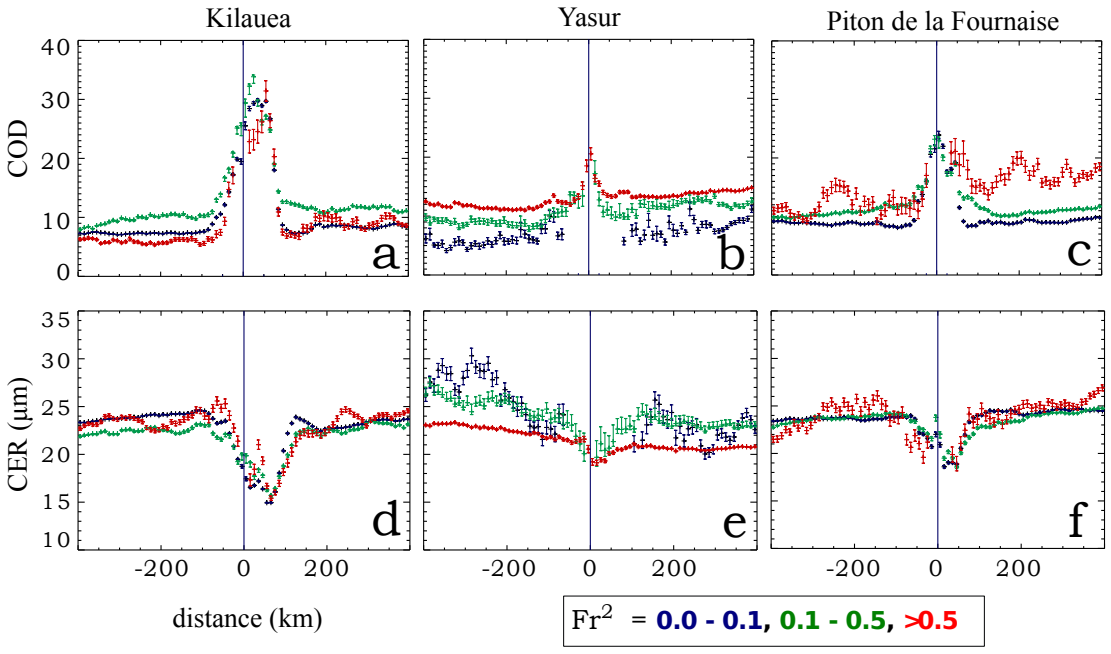

Fig. 10. Profiles showing average COD (a–c) and CER (d–f) at Kīlauea, Yasur and Piton de la Fournaise, separated according to Froude number squared (Fr^2) as estimated from ECMWF data. Fr^2 = 0–0.1 is blue, Fr^2 = 0.1–0.5 is green and Fr^2 >0.5 is red.

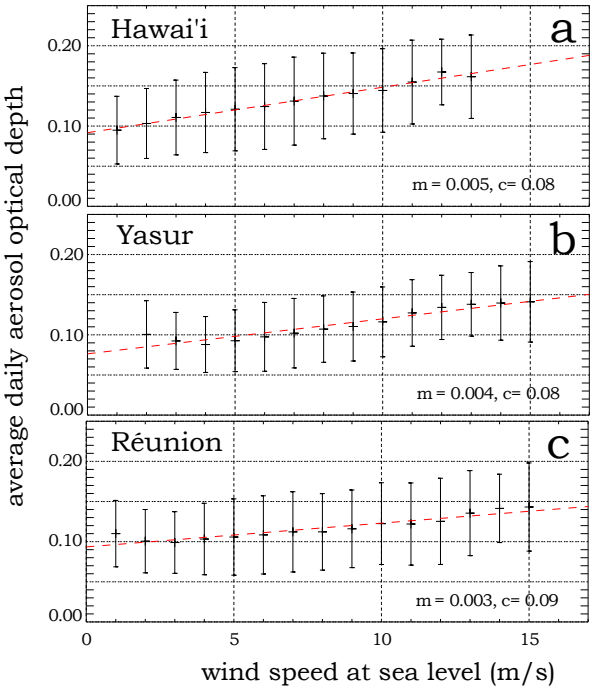

Fig. 11. Daily average AOD at 550 nm measured from MODIS, Aqua between 2002 and 2008 with 50 km of the coasts of a) Hawai'i , b) Yasur and c) Réunion plotted as a function of horizontal wind speed at sea level from ECMWF. Error bars show the standard deviation in AODs for bin intervals of 1 m/s.